NanoScience Technology, Volume 2 (2021), pp: 1-21

NanoScience Technology

Journal homepage: https://jnanoscitec.com

Effects of post-treatment processes on photovoltaic performance and morphology of organic solar cells: A review

H. Zarin Toranj[a], S. Aynehband[a], S. Akbari[a*]

[a] *NanoSciTec GmbH, Hermann Weinhauser str. 67, Munich, 81867, Germany*

Abstract

Organic solar cells (OSCs) have attracted tremendous attention during the last two decades because of their specific properties. Any effort to optimize the performance of OSCs while maintaining their power conversion efficiency (PCE) is of high importance for expanding their applications. One of the most noticeable methods for enhancing the efficiency of the OSCs is tuning their morphology, specifically the active layer morphology. For this purpose, different techniques have been proposed. Post-treatment processes including thermal annealing (TA) and solvent vapor annealing (SVA) treatments are among the most applied and studied procedures. This study aims to give a summary of the paths through which TA and SVA affect the morphology and performance of OSCs by reviewing some of the recent studies in this area.

Keywords: Organic solar cells (OSCs), Morphology, Solvent vapor annealing (SVA), Thermal annealing (TA)

Table of Contents

* Corresponding author: S. Akbari. Tel.: +49-151-664-32106 *E-mail address*: somayeh.akbari@nanoscitec.com

1. Introduction

The crystalline silicon solar cell is the most studied technology in photovoltaics (PV), so the lower cost of silicon solar cells in comparison with organic solar cells (OSCs) is expected because of its long-time industrial production [1]. However, OSCs are considered a low-cost source of renewable energy [2]. In addition, properties such as color tunability, simple device structure, low-cost manufacturing, biocompatibility, low toxicity, and scalability are the reasons for considering OSCs as alternatives for silicon-based solar cells [3-8]. The way to compete with crystalline solar cells is developing the unique characteristics of OSCs by focusing on innovation in their features such as their lightweight properties, semitransparency, and flexibility along with improving their lifetime and the power conversion efficiency (PCE) [1, 9]. In addition, the energy payback times of OSCs, which is defined as the operation time required to regain the energy expended for device fabrication, are considerably shorter than those of single crystalline silicon solar cells [10]. Substantial progress in organic semiconductors results in considerable improvements in the design and application of OSCs, which can be noted by surpassing the PCE of 10% and reaching the PCE of 16% for single-junction OSCs, making them comparable with inorganic solar cells [11, 12]. The benefits of OSCs bulk heterojunction (BHJ), which is made by preparing blends of donors/acceptors, can be shorter exciton diffusion lengths and bicontinuous carrier transport pathways, which lead to remarkable enhancement in exciton dissociation efficiency [13].

For large-scale production, it is vital to gain a multi-perspective view from the film evolution, as it is of important information about the morphology and affects device performance, and this is one of the most influencing approaches in optimization [9, 14-17]. The parameters such as pressure and temperature impact the properties like kinetics and aggregation of the polymers of active layers. Zhao and coworkers [18] evaluated the effect of temperature by applying hot hydrocarbon solvent via slot-die coating for OSCs production using PBDB-T-F:BTP-4F as the active layer. In their study, three solvents of chlorobenzene (CB) at 80 °C, orthoxylene (o-XY) at 100 °C, and 1,2,4-trimethylbenzene (TMB) at 110 °C were used and caused an increase in the PCE of devices to the values of 15%, 15.2%, and 15.2%, respectively. As they reported, although open-circuit voltage (VOC), short-circuit current density (JSC), and fill factor (FF) were improved by increasing the temperature, but temperatures higher than these values resulted in the reduction of the PCE. Some of the reported results related to the effects of SVA and TA on the photovoltaic properties of the OSCs are summarized in Table 1.

Solvent selection, TA, solvent vapor annealing (SVA), ternary strategy, and additives are among the applied morphological control methods which have been proven to be successful methods with promising results showing the enhancement of the device performance [17, 19-25]. Applying high boiling point solvent additives, which extends the drying time, allows the film to reach a thermodynamic equilibrium [5]. SVA and TA of organic photovoltaics (OPVs) are among the most applied post-treatments, and their effects on device performance during film formation have been analyzed; they can be mentioned as the methods to reach acceptable levels of reproducibility, scalability, and tunability [26]. Datt and coworkers [27] compared the PCE of as-cast, vacuum annealed, solvent vapor annealed, and thermal annealed devices. The results, indicated the range of SVA>VA>TA>as-cast for the PCE of the related devices with different acceptors and also the best photovoltaic properties such as the highest FF, V_{OC} and J_{SC} for the SVA-treated device.

The results of Berlinghof and coworkers' study [24] on the post-treatment of DRCN5T:PC71BM blend by SVA showed that the phase purity of DRCN5T increased after SVA. Wang and coworkers [28] investigated the three blend films of D18:Y6-based, D18:IT-4F-based, and D18:IEICO-4Cl-based solar cells and achieved PCEs of 17.6%, 14.9%, and 1.4%, respectively. The low miscibility and the consequent insufficient morphology control of the last item was introduced as the reason for the low PCE. Low external quantum efficiency (EQE) and low FF also proved the morphological problem, which shows too large and too pure domains ending in exciton harvesting losses. Furthermore, Photoluminescence (PL) quenching measurements for these three combinations had been performed. Excellent quenching was observed for the two former cases, but not for the last one, perhaps because of the large and relatively pure domains of both D18 and IEICO-4Cl. In addition, Chen and coworkers [29] used the p-DTS(FBTTh2)2:PC71BM blend as the active layer by SVA and the combination of SVA and TA. It was shown that PCE increased from 2.31% to 7.48%, Voc decreased from 0.79 V to 0.77 V, Jsc enhanced from 8.61 mA cm^{-2} to 14.8 mA cm^{-2}, and FF increased from 34.3% to 65.4%, for as-cast and after SVA treatment, respectively. As it can be observed, PCE, Jsc, and FF increased, while Voc decreased due to lowering the quasi-Fermi levels for

carrier transport because of depleted carrier density [29]. In their study, device parameters after TA following SVA improved to Voc=0.80V, Jsc=15.2mA cm^{-2}, FF=67.7%, and PCE=8.22% which are appealing results and prove the importance of post-treatment methods.

Based on the achieved results related to the effects of SVA and TA on the performance and morphology of OSCs, it can be concluded that these processes play a meaningful role in improving the performance of OSCs. The current paper aims to give a brief review of the effects of these two main post-processing treatments on the morphology and photovoltaic properties of OSCs with a short introduction of the application of supercritical fluids.

2. Post-treatments

Tuning domain crystallinity can be a practical approach for improving device performance in addition to the polymer type and fabrication engineering methods [3]. By studying the morphology of both as-cast and the optimal blend film, the effectivity of annealing methods can be evaluated to enhance and change the nanostructure of the annealed film [30]. Kinetics and thermodynamics, including solubility and miscibility as a result of the disordered regimes, create the complexity of BHJ because of the partial miscibility of the polymers involved [3]. The aforementioned kinetic and thermodynamic parameters affecting the BHJ formation, including the temperature, pressure, vapor pressure of additives, donor and acceptor solubility, crystallization/aggregation properties, interactions between solvents and the donor and acceptor, and the deposition conditions that influence the drying kinetics [5]. Post-treatment by the solvent is helpful for the surface engineering of the active layer and can enhance the morphology and, consequently, device performance by controlling the nanostructure of the blend film [31]. SVA and solubility can help to manage the kinetics and thermodynamics of BHJ arrangement. The molecular ordering and the morphology of blend films determine the charge generation, dissociation, recombination, and transporting properties [28]. By a change in the solvent evaporation rate, temperature can affect the morphology because of its effects on the thermodynamic equilibrium conditions of the polymer and the solvent mixture. Kinetic energy enhancement of polymer chains due to an increase in the temperature leads to a reduction in the agglomeration of polymer chains [9]. On the other hand, the faster evaporation speed at the higher temperature gives less time for growing polymer chains to extend the polymer domains [9]. Therefore, the optical and electronic properties of BHJ can be affected by these variables and can influence their carrier dynamics [3]. The performance of some BHJ blend systems decreases due to overprocessing by long-time TA or excess solvent additive concentrations [5].

The BHJ in a multicomponent solvent system has a complex structure with complicated thermodynamic and kinetic conditions and cannot be explained by a simple mechanism [5]. A balanced crystallinity and miscibility can be achieved by post-treatments, like TA and SVA [8]. For optimizing device efficiency, tuning the crystallinity and the phase purity of the active layer is suggested [24]. SVA and TA lead to increase the domain size and purity enhancement [32]. More importantly, sufficient electron percolating pathways are essential for achieving high performance in OSCs, and reaching a composition of mixed domains near the percolation threshold is vital [28].

Applying supercritical fluids like carbon dioxide (CO2) is one of the less-studied methods for post-treatment. By increasing the pressure and temperature of a fluid above its critical values, the fluid is considered as a supercritical fluid [33]. The density, viscosity, and diffusion of the supercritical fluid in the critical region change by slight variations of temperature and pressure. Supercritical fluids influence the diffusivity of a gas and the density of a liquid. Therefore they make the supercritical phase a promising alternative for conventional and mostly toxic solvents [33, 34]. Supercritical fluids can be used as solvents, antisolvents, or plasticizers, and they have been shown to be used successfully in polymer process applications [33, 35]. The supercritical conditions of CO2 are Tc=304 K, Pc=7.38 Mpa, and it can be removed and recovered by depressurization [33]. Supercritical CO2 (ScCo2) is non-flammable, and non-toxic, with inert characteristics, negligible surface tension, and a high diffusion coefficient, which can be the reason of its high mass transfer [33, 34, 36, 37]. The applicability of ScCO2 as a solvent in polymer applications has been proven for processes such as polymer blending, foaming, and polymerization [33]. ScCO2 has shown its potential as a suitable solvent for nonpolar (and some polar) and low-molecular-weight compounds in comparison with the solvency potential for high-molecular-weight polymers; on the other hand, it is soluble in many molten polymers [33].

Based on the results reported by Yousefi and coworkers [35], crystallinity decreased by increasing the pressure, and it can be due to the solution turbulency enhancement. The effects of ScCO2 on the extraction of the polymer fraction from crystalline

silicon solar cells was studied by Zachmann and coworkers [38]. By reporting the Fourier-transform infrared spectroscopy (FTIR) results, they showed that only ester and ethylaldehydes were extracted from the organic layer. Similarly, Amonoo and coworkers [39] used ScCO2 for post-processing the film containing P3HT/PC61BM. Based on their findings, ScCO2 could be considered as a solvent with a minimal solvency effect on PC61BM, whereas it was a considerable solvent for P3HT [39]. It was discussed that CO2 could change the amorphous regions by increasing the free volume and enhancing the chain mobility after absorption into the polymer, and CO2 is able to rearrange it into a kinetically favored state compared to lower temperature conditions [40].

Among the reported post-treatment methods to manipulate the morphology and, consequently, the photovoltaic properties of OSCs, SVA and TA are two of the most studied procedures. A summary of the path through which these methods affect the morphology and properties of OSCs as well as an overview of the reported photovoltaic properties are presented in the following sections.

2.1 Solvent vapor annealing (SVA)

SVA treatment is done by transferring the blend film to a chamber containing a solvent vapor made out of evaporated solvent without any direct contacts, and the molecules take up the solvents (Figure 1) [41, 42]. In the SVA treatment, the donor and/or acceptor materials can be reorganized by the penetration and diffusion of the solvent vapor into the blend film, and a more thermodynamically favorable morphology in the blend will be achieved by the absorption [19, 26]. In fact, the active layer is exposed to the applied solvent vapor to provide the condition needed for its diffusion into the organics. It is also noteworthy that some factors including the solubility of the active layer's molecules, partial pressure of the solvent, and the applied time are effective on the efficiency of the SVA treatment [43].

Other than the conventional SVA methods, which are putting the substrate into a petri dish [27], Zomerman and coworkers [26] developed an approach by applying different vapor pressures by a flow of wet carrier gas to improve reproducibility. Bell jar, which is performed by evaporation of the solvent in an enclosed box or jar, for producing a concentration gradient of the used solvent, can also be considered as one of the simplest SVA options [26]. Zhang and coworkers [44] studied the effects of upside-down TA (DTA) and SVA (DSVA), and showed an increase in the PCE after these post-processing treatments. They concluded that the enhancement was due to the suitable crystallinity of the donor and the produced purified acceptor domain. It was also explained that the optimized phase separation in the vertical direction because of the gravity and capillary force might be the reasons for the better results. SVA showed promising results in self-assembling of high-molecular-weight polymers or polymers with high interaction parameters. The solvation state makes this process faster in comparison with TA; however, the reproducibility of the film swelling process is hard to control [45]. For solving this problem, different approaches have been proposed. For example, Hulkkonen and coworkers [45]reported applying an automated system for SVA by following preprogrammed annealing profiles to control the film swelling by local heating or cooling based on the information derived from a feedback loop. It was reported that this approach could also shorten the annealing time to less than 15 min.

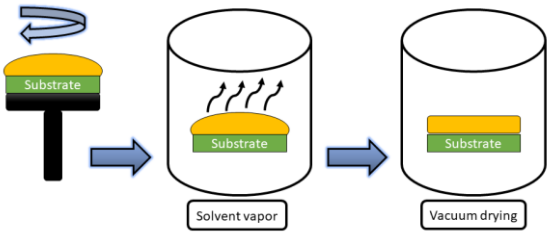

Figure 1. The schematic illustration of solvent vapor annealing (SVA) treatment

The solvents selection can be based on their solubility power for the acceptor, donor, or both of them, as was followed by Berlinghof and coworkers [24]. They reported that the selected solvents for annealing affected the annealing kinetics and, consequently, the required time for that, but they were not so influential on the crystalline structure. When the applied acceptor in the OSC is fullerene, it is sensitive to the SVA time because of its spherical molecular structure, and applying an optimum SVA time is required [23].

The organization of the molecules at a lower energy state and increasing the molecular mobility occur because of the decrease in the glass transition temperature by the SVA treatment, which causes easier translational movement of polymer chains [21, 46, 47]. The solvent vapor penetrates the film, causes thermodynamic rearrangement, and enhances the miscibility, molecular orientation, and conformation [32]. It has been proven that the application of SVA, during- or post-casting the active layer, can substantially enhance its photovoltaic properties for both fullerene and non-fullerene photovoltaic blends [10, 28, 44]. For small-molecule donor-based devices,

solvent–molecular interaction is vital and cannot be achieved easily. It is because of the similar chemical structure and properties of the donor and acceptor, the importance of reaching balanced miscibility and the appropriate phase separation, which is essential for achieving high performance [8, 23, 31, 42, 48].

Controlling the active layer morphology in OPVs is one approach for device performance optimization [21]. In the SVA treatment, phase separation, nucleation, and growth are the dominant processes for the kinetics of the morphology evolution of the small-molecule BHJ blends [21]. The crystallinity of the active layer is one of the determining factors on the charge transport and collection, and it can affect the overall performance of the BHJ OSC [49]. It has been shown that SVA can influence the crystallinity of polymeric donors and acceptors, along with the scale of phase separation between them in BHJ, and it can improve phase purity [16, 19, 42]. SVA had been proved as a method to optimize the film morphology in BHJ OSCs, and because of the relation between SVA with crystallization and carrier effects that are charge generation, transport, recombination, and extraction, this optimization is mainly related to improvements in these areas which can affect PCE and FF [16, 43]. This can mean reaching a bicontinuous network of donor–acceptor, as the charge separation and charge transporting are determined by the interpenetrated networks of the bulk [19, 21, 25].

A suitable solvent with a high vapor pressure crystallizes donor molecules, resulting in increased length scale of phase separation and enhancing the purity of the domain, which can increase the device performance [31]. In contrast, a poor solvent has a lower ability to drive molecules and, consequently, with fewer changes in crystalline content and phase separation [31]. By defining the crystallinity as “the ratio of crystalline fractions to amorphous fractions” based on the definition followed by Berlinghof and coworkers [24], an optimum crystallinity with a focus on the crystallite size is required. It is because high crystallinity ends in high charge carrier mobilities, while large crystallite sizes can affect the separation of the electron-hole-pair [24]. With 20 s of SVA exposure on the BDT[2F]QdC:PC71BM active layer, the change in morphology to a favorable cocontinuous network which is appropriate for charge generation and charge collection processes was observed by Babics and coworkers [43]. However, they reported that increasing the exposure time caused the performance of the device to deteriorate, due to the formation of the domains with sizes greater than the exciton diffusion length, which can affect charge generation [43]. The J-V characteristics of the aforementioned samples subjected to various SVA times and it implies that larger JSC which is 11.4 mA/cm2 and, consequently, the highest PCE which reaches 7.1% is achievable by 20s of SVA [43]. In the Wang and coworkers' study [15], the interpenetrating network by separation of the donor-acceptor phase and the consequent increase in the roughness of the film surface from 0.7 nm without SVA to 1.2 nm and 1.1 nm after 60s and 80s of SVA, respectively, were considered the results of the driving force provided by SVA for facilitating domain grow [15]. In their study, SVA of the device fabricated with NDPPFBT:PC71BM by tetrahydrofuran (THF) vapor and the better solubility of the donor in the solvent caused higher penetration of the solvent into the active layer, led to film morphology tuning, and enhanced the PCE of the device to over 7% [15].

In the study reported by Wang and coworkers [16], the small root-mean-square (RMS) roughness (0.5 nm) of active layers composed of BIT4FTh:PC71BM and BIT4FSe:PC71BM before SVA showed a smooth surface, uniform morphology, and good mixing of the donor with the acceptor. While, after the SVA treatment for 30s with methylene chloride (CH2Cl2), the RMS roughness of 0.8–1.0 nm showed a rougher surface and more phase separation. They concluded that SVA with this solvent could form a good interpenetrating network. In the same study, by using the combination of BIT4FFu:PC71BM, a reduction in the RMS roughness from 3.2 nm to 1.5 nm after SVA was observed, which can be inappropriate for exciton diffusion/dissociation, and consequently, a lower Jsc was achieved by SVA. On the other hand, they reported phase separation and a bicontinuous interpenetrating network with domain sizes of 15–20 nm and 20–25 nm for BIT4FTh:PC71BM and BIT4FSe:PC71BM, respectively, which are favorable for exciton diffusion/dissociation and charge transport [16]. In addition, the efficient exciton separation and charge collection efficiency because of the SVA treatment reported by Jiao and coworkers could increase the Jsc of the solar cell [23].

Li and coworkers [21] applied four different annealing solvents, carbon disulfide (CS2), chloroform (CHCl3), tetrahyrofuran (THF) and methylene chloride (CH2Cl2), to study their impacts on the morphology of the active layer. They concluded that solvent molecules caused the mobility of both the acceptor and the donor, which affected the molecule crystallization. They also showed that the better solubility power of the solvent for the acceptor and donor led to better improvement in device performance, and those with higher solubility and a lower boiling point were the best in morphology control. They reported that the crystal size of PC71BM, which increased with SVA

time, showing the importance of PC71BM aggregation in enhancing device performances. Li and coworkers [21] explained that the increase in the length scale of phase separation and the improved domain purity could be beneficial for the charge transport and collection. It could be the reason for the reduction in charge recombination, and consequently could lead to device performance improvement, regarding the fact that the length scale of phase separation was near the exciton diffusion length [21].

Improvement in hole and electron mobilities has also been reported after SVA. The hole and electron mobilities of the device fabricated based on BIT4FSe increased from 2.7×10−5cm2V-1s-1 to 3.3×10−4cm2V-1s-1, and from 1.4×10−4cm2V-1s-1 to 1.5×10−4cm2V-1s-1 after SVA for 30 s, in the study conducted by Wang and coworkers [16]. They explained that SVA increased the hole mobility and caused a better-balanced hole and electron mobility, which resulted in a higher charge-carrier extraction efficiency, and could be considered the reason for their high FF. In their study, the lower charge-recombination losses led to an increase in FF from 0.48–0.62 before SVA to 0.70–0.75 after SVA by CH2Cl2 for 30 s.

Wang and coworkers [15] reported an increase in the hole mobility of the device fabricated by NDPPFBT which was SVA-treated with CH2Cl2 for 30 s from 5.66×10-6 cm2V-1s-1 to 3.94×10-5 cm2V-1s-1 and further enhancement to 2.40×10-4 cm2V-1s-1 by increasing the time to 60 s. Furthermore, the electron mobility increased from 1.26×10-4 cm2V-1s-1 to 1.67×10-4 cm2V-1s-1 after SVA for 60 s. The resulting better-balanced charge carrier mobility, in this study, caused the FF improvement which reaches 0.73 [15]. As the carrier mobilities of electron and hole, and their ratio are related to the accumulation of space charges and recombination of charge carriers, they explained that enhancement in Jsc and performance of the devices were due to SVA which results in better charge transport, and less charge recombination loss.

Radford and coworkers [50] used PBDBT:ITIC as the active layer compounds and examined the effects of different vapor pressures of 50%, 75%, and 95% of solvent concentration during SVA. They got the noticeable increase in PCE (22%) at 75% solvent concentration. Based on their reported results, SVA treatment of these active layers showed crystallization of the ITIC at the expense of PBDB-T crystallinity; to reach the best balance, the 75%-annealed sample had been proposed to the best ordering of the ITIC acceptor [50]. In this study, a drop in Jsc with film swelling during annealing is reported, and it is due to the reduction in the probability of intermolecular charge transfer. Additionally, they reported that the FF had been improved as a result of the better balancing of the electron and hole mobilities [50].

Solvent annealing in all-polymer systems, like PNDISHD:PBDTT-FTTE, shows slow organization or crystallization process by solvent annealing with chlorobenzene (CB) via producing a more suitable bulk morphology. This phenomenon indicates easier charge separation and less edge-on oriented polymer chains which facilitate carrier mobility [31]. Wang and coworkers [28] showed that SVA was able to enhance molecular ordering in the blended-films of D18:IT-4F and D18:IEICO-4Cl; however, it could affect the D18:Y6 blend only slightly . In another study, Datt and coworkers [27] investigated the device performance and compared the effect of the SVA post-treated substrate with the vacuum annealed treatment on PCE. According to their results, the SVA-treated and the vacuum annealed films increased PCE of the device from 8.6% to 9.7%, respectively, and SVA could enhance PCE for the used small molecule non-fullerene acceptor. Facilitating the formation of a fine, self-organized interfacial layer between the BHJ layer and the electrode is also reported, which could yield the enhancement of PCE for cases with SVA in comparison with the cases without SVA [6].

2.2 Thermal annealing (TA) and the combination of TA and SVA

To attain an acceptable morphology of the active layer, different techniques can be considered. One of the most noticeable ones is applying post-treatments and manipulating the drying process by procedures such as TA which its schematic illustration is shown in Figure 2 [14]. TA has been applied for both of polymer-based PVs and small molecule-based PVs [51]. For example, Sánchez and coworkers [25] showed that when inverted polymer solar cells are fabricated at 100 °C, the performance of the device is dependent on the thickness of the applied active layer, PBDB-T:IT-M, whereas this dependency is less determining for the device which is annealed at 160 °C. The achieved results by Qiu and coworkers [48] revealed that the TA treatment could effectively improve the photovoltaic performance of the small molecule-OSCs, which was considered as the result of changes in the morphology of the active layer after TA. They reported an enhancement in both the hole and electron mobilities after the TA treatment and the appropriate interpenetrating network of the acceptor and donor, leading to the effective exciton dissociation and charge transportation. The increase in hole mobilities due to

SVA and TA+SVA treatments was also observed by Wang and coworkers [52], which the increase in the combined process was larger.

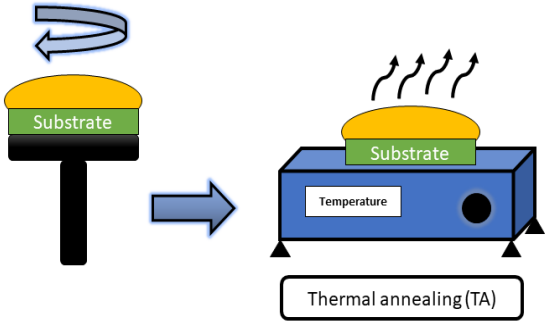

Figure 2. Schematic of the thermal annealing (TA) process

TA could reorganize some P3HT molecules chains presented in amorphous forms and in the P3HT:PCBM matrix to the crystalline forms [53]. The clusters of PCBM, which were shaped with different dimensions in the P3HT:PCBM matrix, prevented orderly dispersing and orientation of the P3HT molecular chains [53]. Wang and coworkers [52] investigated SVA followed by TA on BIT4F, BIT8F, and BIT10F with PC71BM blends, and the results showed both SVA and SVA+TA could result in the enhancement of the donor/acceptor molecular interaction and crystalline order in the films. They reported that SVA or TA+SVA allowed the movement of the molecules and, consequently, the crystalline content of the film and phase separation could change [52]. They had concluded from the uniform TEM image in SVA+TA treatment that TA could lead to better bicontinuous morphology and, consequently, to an increase in FF and PCE. On the other hand, they showed that SVA promoted the mobility of donor molecules. The more crystalline content and enlarged crystal size were achieved as the result of nucleation and growth, and the combined processes ended in favorable crystal sizes. Accordingly, the resulting effective crystalline morphology improved charge carrier transport and charge collections [52]. Besides, Abdullah and coworkers [54] studied the effect of TA treatment at 70 °C for 30 min for one and two times on the device fabricated based on the PCDTBT:PC71BM blend. Based on their results, efficiency decreased upon conducting TA from 9.3% to 4.8% and 2.3% before TA and after one and two times of annealing, respectively, but the stability increased after TA. By annealing the active layers made of P3HT:PCBM above the transition temperature, the amorphous aggregate structure with cavities between their structures was converted into crystallites with lower specific volume and had led to a reduction in the amorphous P3HT:PCBM matrix [53]. Therefore, the volume occupied by water and oxygen molecules decreased [53].

Domain purity due to TA improved to a lesser extent against SVA treatment, which showed that TA could cause higher molecular ordering in films in comparison with SVA, though this observation was not totally acceptable by the observed topography images in Min and coworkers' study [3]. In another study [8], after TA of BSCl:IDIC-4Cl as the active layer, at 120 °C for 10 min, PCE, Jsc, and FF improved, and Voc decreased to the values of 10.57%, 19.1 mA cm-2, 65.6%, and 0.845 V, respectively, while PCE, Voc, Jsc, and FF for the as-cast device were 2.35%, 0.900V, 7.7 mA cm-2, and 33.9%, respectively. In this work, a decrease in donor packing ability after SVA with a stronger molecular crystalline by TA were reported. As a result, they concluded that SVA after TA could enhance the molecular miscibility of the donors and acceptors.

Furthermore, Zhang and coworker [55] studied the effects of TA on the PffBT4T-2OD:PC71BM blend film. They concluded that the existence of the longer exciton diffusion length and, consequently, the larger size of the PffBT4T-2OD domains meaning a reduction in exciton dissociation efficiency of the donor. Their conclusion was based on the achieved longer PL decay lifetime, assuming that the diffusion coefficient of the PffBT4T-2OD excitons was constant and the exciton dissociation probability at the interface did not change after annealing. An appropriate phase separation is required for a promoted charge transport and limiting the carrier recombination loss of polymer solar cells [55]. After TA treatment of a PffBT4T-2OD:PC71BM blend film, due to the disarrangement caused in the originally ordered PffBT4T-2OD, the probability of the movement of photogenerated PffBT4T-2OD+ from the interface would be lower and could lead to an increase in the bimolecular recombination [55].

For any given annealing time, optimum temperature determination for TA is required [53]. In the study conducted by Yi and coworkers [51], by TA treatment of the film comprising solution-processable small molecule (DRDTSBDTT) at 80 °C, a more suitable interpenetrating network was observed with the phase separation and, by annealing at higher temperatures, both the crystal size and the phase separation became larger, which indicates a better interpenetrating network [51]. This observation seemed unfavorable for the exciton diffusion to the donor–acceptor interface, while it could be effective for the separated free charge transporting to the electrode [51].

Improved hole mobility is reported due to the self-organization of conjugated polymers from the TA treatment of the active layer [56]. Traps of electrons and holes in the donor–acceptor interface caused by defects could be decreased by structural improvements in the active layer, and decreases in the traps could lead to the increase in the number of charge carriers [53]. In addition, barrier for holes in the P3HT caused by the amorphous and irregular regions could be decreased, which results in the mobility enhancement of the holes, and annealing of the electrodes could increase the contact surface to the electrodes and the active layer [53]. TA could lead to the smoother surface of the blend film, which means a better contact with the electrode and charge collection efficiency improvement [56].

It has been reported that TA treatment can cause more charge extraction from the OSCs, which is related to the enhanced light absorption, better exciton separation, and/or charge collection efficiency [56]. Likewise, this treatment can increase the Jsc and, consequently, the PCE of solar cells [56]. It was also reported by Wan and coworkers [56] that TA caused more efficient percolation channels and, Jsc, charge separation and collection efficiency increment [56].

On the other hand, impedance spectroscopy in Sánchez and coworkers' research [25], implies that the charge-transfer in the bulk layer was increased by annealing at 160 °C, while, by decreasing the annealing temperature to 100 °C, lower charge-transfer resistance through involved layers in the charge extraction was observed. Facilitation in the efficient exciton dissociation and charge transport could be considered as the main reasons of improving the EQE after TA followed by SVA treatment [29]. Chen and coworkers [29] reported that charge collection efficiency and the charge transport property were improved after SVA and TA treatments, ending in reduced bimolecular recombination loss and, consequently, enhancing Jsc and FF [29]. The study of Sánchez and coworkers [25] revealed that recombination losses were controlled by non-geminate recombination mechanisms when the device was annealed at 160 °C, whereas, by annealing at 100 °C, recombination losses were mostly because of band-tail trap states [25]. In addition, Wang and coworkers [52], concluded that the better charge transport and less charge recombination loss led to the increase in FF after SA or TA+SVA [52].

Table 1. The effects of SVA post-treatment on photovoltaic properties

Active layer compounds	BHJ/Active layer	Processes	Voc (V)	Jsc (mA/cm2)	FF (%)	PCE (%)	Reference
Glass/ITO/ PEDOT:PSS/ Active layer/Al	DRCN5BT-HH:PC61BM	SVA(0s)	0.99	0.19	0.26	0.05	[22]
	DRCN5BT-HH:PC61BM	SVA(60s)	1.10	4.45	0.67	3.26	
	DRCN5BT-TT:PC61BM	SVA(0s)	0.95	1.01	0.38	0.37	
	DRCN5BT-TT:PC61BM	SVA(60s)	0.94	0.79	0.42	0.31	
ITO/PEDOT:PSS/ Active layer/Ca/Al	BDT[2F]QdC: PC71BM	SVA (0s) (CF)	0.96	6.9	33	2.2	[43]

	BDT[2F]QdC:PC71BM	SVA(5s) (CF)	0.95	9.5	38	3.4	
	BDT[2F]QdC:PC71BM	SVA(20s) (CF)	0.94	11.4	66	7.1	
	BDT[2F]QdC:PC71BM	SVA(60s) (CF)	0.94	5.5	58	3.1	
	BDT[2F]QdC:PC71BM	SVA(120s) (CF)	0.94	2.1	36	0.7	
ITO-covered glass/PEDOT:PSS/ Active layer/ Calcium/Aluminum	DRCN5T: PC71BM	As-cast	1.007	6.8	46	3.1	[24]
	DRCN5T: PC71BM	SVA($CHCl_3$)	0.93	12.3	63	7.3	
	DRCN5T: PC71BM	SVA(THF)	0.939	11.9	63	7.0	
	DRCN5T: PC71BM	SVA(CS_2)	0.93	12.4	60	7.0	
ITO/PEDOT:PSS/ Active layer/PFN/Al	p-DTS(FBTTh2)2 : PC71BM	As-cast	0.79	8.61	34.3	2.31	[29]
		SVA (DCM)	0.77	14.8	65.4	7.48	
		SVA+TA	0.80	15.2	67.7	8.22	
ITO/Zn/Active layer /MoO3/Ag	PTB7-T: BAF-4CN	As-cast	0.889	14.2	57.7	7.3 (7.1)	[27]
	PTB7-T: BAF-4CN	SVA(CB),(DIO),(1-Chloronaphthalene)	0.898	15.8	68.1	9.7 (9.5)	
	PTB7T: PC71BM	SVA(CB),(DIO),(1-Chloronaphthalene)	0.791	12.9	57.5	5.9 (5.7)	

ITO/PEDOT:PSS/ Active layer/PDIN/Al	PM7:IT4Cl	As-cast	0.879 ± 0.002	18.89 ± 0.46	68.64 ± 1.53	11.73 ± 0.11	[23]
	PM7:IT4Cl	SVA(CH_2Cl_2)	0.870 ± 0.003	20.19 ± 0.40	70.95 ± 1.68	12.87 ± 0.14	
	PM7:IT4Cl	SVA($CHCl_3$)	0.873 ± 0.002	20.22 ± 0.35	70.52 ± 1.88	12.90 ± 0.08	
	PM7:IT4Cl	SVA(THF)	0.859 ± 0.004	20.23 ± 0.44	71.06 ± 1.76	12.75 ± 0.12	
	PM7:IT4Cl	SVA(CS_2)	0.867 ± 0.004	20.39 ± 0.33	75.63 ± 1.13	13.58 ± 0.09	
ITO/ PEDOT:PSS/ Active layer/Al	VC89:PC71BM	As cast	0.96	9.28	52	4.63	[49]
	VC89:PC71BM	As cast + SA(DIO, 3% vol)	0.92	10.96	60	6.05	
	VC89:PC71BM	SVA with (CF/DIO)	0.92	11.68	62	6.66	
ITO/PDEDOT:PSS/ Active layer/Al	DR3TBDTT: PC71BM/PrC 60 MA	As-cast	0.918	12.95	66.7	7.66	[21]
	DR3TBDTT: PC71BM/PrC 60 MA	SVA(CH_2Cl_2)	0.889	13.55	71.7	8.30	
	DR3TBDTT: PC71BM/PrC 60 MA	SVA(THF)	0.893	13.38	69.3	8.14	
	DR3TBDTT: PC71BM/PrC 60 MA	SVA($CHCl_3$)	0.881	13.84	74.8	9.00	
	DR3TBDTT:	SVA(CS_2)	0.886	14.21	76.1	9.36	

	PC71BM/PrC 60 MA						
ITO/ZnO/BHJ/MoOx (10 nm)/Ag (100 nm)	P3HT: PDI-DPP-PDI	As-cast	0.80	0.62	26.8	0.13 (0.14)	[57]
		SVA(4min)(CF)	0.68	2.78	34.5	0.65 (0.68)	
	PCDTBT: PDI-DPP-PDI	As-cast	1.03	1.46	26.6	0.40 (0.43)	
		SVA(8min)(CF)	1.05	3.64	37.9	1.45 (1.53)	
	PDTT-BOBT: PDI-DPP-PDI	As-cast	1.01	4.79	33.5	1.62 (1.67)	
		SVA(4min)(CF)	0.99	8.61	44.1	3.76 (3.90)	
ITO/TiOx/Active layer /V2O5/Ag	PBDB-T: IT-M	TA(100◦C)(110nm active layer)	0.847	14.94	59.40	7.52	[25]
	PBDB-T: IT-M	TA(100◦C) (106nm active layer)	0.845	15.38	60.22	7.93	
	PBDB-T: IT-M	TA(100◦C) (102nm active layer)	0.857	16.10	61.59	8.50	
	PBDB-T: IT-M	TA(100◦C) (91 nm active layer)	0.87	16.14	64.26	9.02	
	PBDB-T: IT-M	TA(160◦C) (111nm active layer)	0.872	15.20	60.70	8.05	
	PBDB-T: IT-M	TA(160◦C) (105 nm active later)	0.878	15.25	60.50	8.10	
	PBDB-T: IT-M	TA(160◦C) (100 nm active layer)	0.878	15.18	60.50	8.07	
	PBDB-T:	TA(160◦C) (88 nm active layer)	0.87	15.32	62.12	8.28	

	IT-M						
ITO/PEDOT:PSS/ Active layer/PFN/Al	DPPFB: PC71BM	As cast	0.84	7.14	38.77	2.31	[15]
	DPPFB: PC71BM	SVA(30 s)(CH_2Cl_2)	0.76	9.88	69.00	5.21	
	DPPFB: PC71BM	SVA(50 s)(THF)	0.79	5.80	65.89	3.03	
	DPPFBT: PC71BM	As cast	0.81	8.71	49.58	3.51	
	DPPFBT: PC71BM	SVA(30s)(CH_2Cl_2)	0.76	10.51	60.85	4.83	
	NDPPFBT: PC71BM	As cast	0.92	9.38	54.04	4.67	
	NDPPFBT: PC71BM	SVA(30s)(CH_2Cl_2)	0.88	11.00	63.03	6.05	
	NDPPFBT: PC71BM	SVA(50 s)(THF)	0.89	9.52	68.97	5.84	
	NDPPFBT: PC71BM	SVA(60 s)(THF)	0.88	10.71	71.60	6.86	
ITO/PEDOT:PSS/ Active layer/PFN/Al	BIT4FFu: PC71BM(1:3)	As-cast	0.90	11.20	53	5.34	[16]
ITO/PEDOT:PSS/ Active layer/PFN/Al	BIT4FFu: PC71BM(1:3)	SVA(30s)(CH_2Cl_2)	0.83	5.34	71	3.11	
ITO/PEDOT:PSS/ Active layer/PFN/Al	BIT4FFu: PC71BM(1:2)	As-cast	0.89	11.12	61	6.01	
ITO/PEDOT:PSS/Active layer/PFN/Al	BIT4FFu: PC71BM(1:2)	SVA(30s)(CH_2Cl_2)	0.84	8.12	74	5.03	
ITO/PEDOT:PSS/	BIT4FTh:	As-cast	0.94	11.73	60	6.65	

Active layer/PFN/Al	PC71BM(1:3)						
ITO/PEDOT:PSS/ Active layer/PFN/Al	BIT4FTh: PC71BM(1:3)	SVA(30s)(CH_2Cl_2)	0.89	11.68	75	7.83	
ITO/PEDOT:PSS/ Active layer/PFN/Al	BIT4FTh: PC71BM(1:2)	As-cast	0.94	12.02	62	7.00	
ITO/PEDOT:PSS/ Active layer/PFN/Al	BIT4FTh: PC71BM(1:2)	SVA(30s)(CH_2Cl_2)	0.89	13.06	75	8.70	
ITO/PEDOT:PSS/ Active layer/PFN/Al	BIT4FSe: PC71BM(1:3)	As-cast	0.91	11.36	49	5.07	
ITO/PEDOT:PSS/ Active layer/PFN/Al	BIT4FSe: PC71BM(1:3)	SVA(30s)(CH_2Cl_2)	0.87	13.40	72	8.41	
ITO/PEDOT:PSS/ Active layer/PFN/Al	BIT4FSe: PC71BM(1:2)	As-cast	0.91	11.09	48	4.88	
ITO/PEDOT:PSS/ Active layer/PFN/Al	BIT4FSe: PC71BM(1:2)	SVA(30s)(CH_2Cl_2)	0.86	12.64	71	7.74	
ITO/PEDOT:PSS/ Active layer/PFN/Al	BIT4F: PC71BM	As-cast	0.94	10.86	60.61	6.19	[52]
	BIT4F: PC71BM	SVA(CH_2Cl_2)	0.89	12.20	75.33	8.16	
	BIT4F: PC71BM	TA+SVA(CH_2Cl_2)	0.89	12.25	76.30	8.27	
	BIT6F: PC71BM	As-cast	0.91	11.61	60.19	6.34	
	BIT6F:	SVA(CH_2Cl_2)	0.89	11.41	73.38	7.63	

	PC71BM						
	BIT6F: PC71BM	TA+SVA(CH_2Cl_2)	0.91	12.97	73.11	8.66	
	BIT8F: PC71BM	As-cast	0.88	10.57	56.05	5.23	
	BIT8F: PC71BM	SVA(CH_2Cl_2)	0.88	10.29	65.38	5.93	
	BIT8F: PC71BM	TA+SVA(CH_2Cl_2)	0.89	10.90	69.07	6.67	
	BIT10F: PC71BM	As-cast	0.92	11.62	58.99	6.30	
	BIT10F: PC71BM	SVA(CH_2Cl_2)	0.92	11.38	61.30	6.39	
	BIT10F: PC71BM	TA+SVA(CH_2Cl_2)	0.91	11.72	65.78	7.04	
	PBITnF: PC71BM	As-cast	0.87	6.22	54.65	.96	
	PBITnF: PC71BM	SVA(CH_2Cl_2)	0.87	5.76	57.65	3.10	
	PBITnF: PC71BM	TA+SVA(CH_2Cl_2)	0.89	8.64	55.31	4.23	
ITO/PEDOT:PSS/ Active layer/	D18:Y6	As-cast	0.843	23.97	76.4	15.42 ± 0.26	[28]
	D18:Y6	SVA(CF)	0.837	27.14	76.1	17.31 ± 0.21	

PFN-Br/Ag	D18:IT-4F	As-cast	0.896	20.25	68.6	12.46 ± 0.38	
	D18:IT-4F	SVA(CF)	0.864	22.27	74.6	14.37 ± 0.36	
	D18:IEICO-4Cl	As-cast	0.798	3.24	49.1	1.27 ± 0.04	
	D18:IEICO-4Cl	SVA (CF)	0.796	3.45	49.1	1.35 ± 0.06	
ITO/PEDOT:PSS/ Active layer/LiF/Al (A-D-A type oligothiophenes1-6)	oligomer 1: PC61BM (1:2)	SVA (0s)	0.829	8.8	66	4.32 (±0.18)	[19]
		SVA (30s) ($CHCl_3$)	0.821	8.9	63	3.97 (±0.30)	
	oligomer 2: PC61BM (1:2)	SVA (0s)	0.820	8.3	56	3.47 (±0.18)	
		SVA (30s) ($CHCl_3$)	0.810	10.5	66	4.60 (±0.47)	
	oligomer 3: PC61BM (1:2)	SVA (0s)	0.837	7.1	64	3.09 (±0.33)	
		SVA (30s) ($CHCl_3$)	0.840	8.4	66	3.48 (±0.51)	
	oligomer 4: PC61BM (1:2)	SVA (0s)	0.797	5.4	28	0.31 (±0.27)	
		SVA (30s) ($CHCl_3$)	0.829	8.2	65	3.23 (±0.70)	
	oligomer 5: PC61BM (1:1)	SVA (0s)	0.865	8.00	44	2.26 (±0.57)	
		SVA (30s) ($CHCl_3$)	0.841	11.4	63	5.13 (±0.47)	
	oligomer 6: PC61BM (1:2)	SVA (0s)	0.817	4.1	32	0.94 (±0.09)	
		SVA (30s) ($CHCl_3$)	0.843	10.1	72	5.59 (±0.28)	
ITO/PEDOT:PSS/ Active layer/MoO3/Al	ZnP2-DPP: PC61BM	As-cast	0.80	6.58	31.02	1.60	[42]
	ZnP2-DPP: PC61BM	SVA(CF)	0.64	19.23	67.04	8.36	
	ZnP2-DPP:	SVA(CH_2Cl_2)	0.63	17.72	57.36	6.50	

	PC61BM						
	ZnP2-DPP: PC61BM	SVA(CS_2)	0.64	20.52	69.14	9.22	
	ZnP2-DPP: PC61BM	SVA(THF)	0.70	9.11	66.20	4.32	
ITO/PEDOT:PSS/ Active layer/Al	DRDTSBDTT/ PC71BM	TA (60°C)	0.994	8.99	44.8	4.00	[51]
		TA (80°C)	0.975	10.08	51.3	5.05	
		TA (100°C)	0.966	8.96	48.2	4.17	
		TA (120°C)	0.956	8.02	47.4	3.63	
Glass/ITO/ PEDOT:PSS/Active layer/PFN/Al	DRCN5T: PC71BM	As-cast	0.99	7.40	49.6	3.55	[44]
		TA	0.93	14.62	59.4	7.82	
		DTA	0.93	15.07	60.0	8.23	
		DTA+DSVA	0.91	15.77	63.5	9.01	
ITO/ZnO/Active layer/MoO3/Ag	PTB7-Th:ITIC	As-cast	0.805	13.21	58.18	6.25±0.15	[4]
		SC-SVA(CF)	0.817	14.15	64.72	7.51±0.13	
ITO/ ZnO/Active layer/ MoO3/Ag	PffBT4T-2OD: PC71BM	As-cast	0.73	21.92	60	9.50 ± 0.23	[55]
		TA (80°C)	0.75	16.97	59	7.46 ± 0.13	
		TA (150°C)	0.76	15.32	0.57	6.62 ± 0.14	
ITO/ZnO (35 nm)/Active layer / MoO3 (10 nm)/ Al (100 nm)	PCBSD (20 nm)/DR3TBDTT (30 nm)	As spin- coated	0.67	2.5	0.36	0.64	[58]
		SVA(CS_2)	0.64	3.7	0.45	1.1	

ITO/PEDOT:PSS/ Active layer/MoOx/Ag	BSCl: IDIC-4Cl	As-cast	0.90	7.7	33.9	2.32±0.024	[8]
		SVA (THF)	0.92	12.9	45.6	5.10±0.39	
		TA	0.84	19.1	65.6	10.29±0.206	
		SVA(THF) +TA	0.86	21.5	70.0	12.85±0.178	
ITO/ZnO/ Active layer/MoO3/Ag	PTB7: PC71BM	As-cast	0.68	15.81	61.1	6.55	[59]
	PTB7: PC71BM	SVA (5min) (Methanol)	0.69	16.14	63.7	7.11	
	PTB7: PC71BM	SVA (10min) (Methanol)	0.71	16.50	62.2	7.34	
	PTB7: PC71BM	SVA (15min) (Methanol)	0.73	16.62	66.2	8.13	
	PTB7: PC71BM	SVA (20min) (Methanol)	0.72	16.13	65.4	7.58	
	PTB7: PC71BM	SVA (30min) (Methanol)	0.72	15.72	64.1	7.23	
	PTB7: PC71BM	SVA (10min) (Ethanol)	0.71	17.32	63.2	7.71	
	PTB7: PC71BM	SVA (10min) (DMSO)	0.70	17.41	63.1	7.72	
	PTB7: PC71BM	SVA (10min) (Acetone)	0.70	16.24	64.6	7.37	
	PTB7: PC71BM	SVA (10min) (IPA)	0.71	15.33	60.5	6.60	

Carbon disulfide (CS2), Chlorobenzene (CB), Chloroform (CF) (CHCl3), Dichloromethane (DCM), 1,8-Diiodooctane (DIO), Dimethylsulfoxide (DMSO), Isopropanol (IPA), Methylene chloride (CH2Cl2), Poly(3,4-ethylenedioxythiophene):polystyrene sulfonate (PEDOT:PSS), Solvent additive (SA), Spin-coating (SC), Tetrahydrofuran (THF)

3. Conclusion

OSCs are finding their way to the market. To pave the way, enhancement in their performance is necessary. Post-treatment processes such as TA and SVA are applied to enhance the performance and even the stability of photovoltaic devices through improving the morphology of the layers, particularly the active layer. Based on the reported studies, it can be concluded that the effectivity of the SVA and TA post-treatments differs based on various parameters, including the molecular structure of the involved layer. Solvent selection in SVA treatment and temperature in the TA treatment, in addition to tuning the time of the process, are essential in achieving the best results. By improving the crystallinity and tuning the purity of the phases, TA and SVA can affect the photovoltaic properties of the devices. In this paper, we have tried to give a brief description of how the enhancement originated from SVA and TA affects the performance of OSCs by reviewing the research studies conducted during around last decade.

4. References

1. M. Riede, D. Spoltore, K. Leo, Organic Solar Cells—The Path to Commercial Success, Advanced Energy Materials, 2002653, 11 (2021).
2. O.O. Amusan, H. Louis, S.-u. Zafar, A.T. Hamzat, D.M. Peter, Different interface engineering in organic solar cells: a review, Chemical Methodologies, 425-441, 3 (2019).
3. J. Min, N.S. Güldal, J. Guo, C. Fang, X. Jiao, H. Hu, T. Heumüller, H. Ade, C.J. Brabec, Gaining further insight into the effects of thermal annealing and solvent vapor annealing on time morphological development and degradation in small molecule solar cells, Journal of Materials Chemistry A, 18101-18110, 5 (2017).
4. L. Zhang, B. Lin, Z. Ke, J. Chen, W. Li, M. Zhang, W. Ma, A universal approach to improve electron mobility without significant enlarging phase separation in IDT-based non-fullerene acceptor organic solar cells, Nano Energy, 609-617, 41 (2017).
5. C. McDowell, M. Abdelsamie, M.F. Toney, G.C. Bazan, Solvent Additives: Key Morphology-Directing Agents for Solution-Processed Organic Solar Cells, Advanced Materials, 1707114, 30 (2018).
6. Y. Lin, L. Yu, Y. Xia, Y. Firdaus, S. Dong, C. Müller, O. Inganäs, F. Huang, T.D. Anthopoulos, F. Zhang, One - Step Blade - Coated Highly Efficient Nonfullerene Organic Solar Cells with a Self - Assembled Interfacial Layer Enabled by Solvent Vapor Annealing, Solar RRL, 1900179, 3 (2019).
7. D. Yang, F.C. Löhrer, V. Körstgens, A. Schreiber, B. Cao, S. Bernstorff, P. Müller - Buschbaum, In Operando GISAXS and GIWAXS Stability Study of Organic Solar Cells Based on PffBT4T-2OD: PC71BM with and without Solvent Additive, Advanced Science, 2001117, 7 (2020).
8. Z. Zhang, Q. Wu, D. Deng, S. Wu, R. Sun, J. Min, J. Zhang, Z. Wei, The post-treatment effects on open circuit voltages and device performances in a high efficiency all-small-molecule organic solar cell, Journal of Materials Chemistry C, 15385-15392, 8 (2020).
9. K.S. Wienhold, C.L. Weindl, S. Yin, T. Tian, M. Schwartzkopf, A. Rothkirch, S.V. Roth, P. Müller-Buschbaum, Following in situ the evolution of morphology and optical properties during printing of thin films for application in non-fullerene acceptor based organic solar cells, ACS applied materials & interfaces, 40381-40392, 12 (2020).
10. C. Yan, S. Barlow, Z. Wang, H. Yan, A.K.-Y. Jen, S.R. Marder, X. Zhan, Non-fullerene acceptors for organic solar cells, Nature Reviews Materials, 1-19, 3 (2018).
11. A. Classen, T. Heumueller, I. Wabra, J. Gerner, Y. He, L. Einsiedler, N. Li, G.J. Matt, A. Osvet, X. Du, Revealing hidden UV instabilities in organic solar cells by correlating device and material stability, Advanced energy materials, 1902124, 9 (2019).
12. C. Liu, X. Du, S. Gao, A. Classen, A. Osvet, Y. He, K. Mayrhofer, N. Li, C.J. Brabec, A Cross-Linked Interconnecting Layer Enabling Reliable and Reproducible Solution-Processing of Organic Tandem Solar Cells, Advanced Energy Materials, 1903800, 10 (2020).
13. Y. Xu, H. Yao, L. Ma, J. Wang, J. Hou, Efficient charge generation at low energy losses in organic solar cells: a key issues review, Reports on Progress in Physics, 082601, 83 (2020).
14. C. Lin, E.Y. Lin, F.Y. Tsai, Enhanced Thermal Stability and Efficiency of Polymer Bulk-Heterojunction Solar Cells by Low-Temperature Drying of the Active Layer, Advanced Functional Materials, 834-839, 20 (2010).
15. J.-L. Wang, Z. Wu, J.-S. Miao, K.-K. Liu, Z.-F. Chang, R.-B. Zhang, H.-B. Wu, Y. Cao, Solution-processed diketopyrrolopyrrole-containing small-molecule organic solar cells with 7.0% efficiency: in-depth investigation on the effects of structure modification and solvent vapor annealing, Chemistry of Materials, 4338-4348, 27 (2015).

16. J.L. Wang, F. Xiao, J. Yan, Z. Wu, K.K. Liu, Z.F. Chang, R.B. Zhang, H. Chen, H.B. Wu, Y. Cao, Difluorobenzothiadiazole-Based Small-Molecule Organic Solar Cells with 8.7% Efficiency by Tuning of π - Conjugated Spacers and Solvent Vapor Annealing, Advanced Functional Materials, 1803-1812, 26 (2016).
17. W. Deng, K. Gao, J. Yan, Q. Liang, Y. Xie, Z. He, H. Wu, X. Peng, Y. Cao, Origin of reduced open-circuit voltage in highly efficient small-molecule-based solar cells upon solvent vapor annealing, ACS applied materials & interfaces, 8141-8147, 10 (2018).
18. H. Zhao, H.B. Naveed, B. Lin, X. Zhou, J. Yuan, K. Zhou, H. Wu, R. Guo, M.A. Scheel, A. Chumakov, Hot Hydrocarbon-Solvent Slot-Die Coating Enables High-Efficiency Organic Solar Cells with Temperature-Dependent Aggregation Behavior, Advanced materials, 2002302, 32 (2020).
19. C.D. Wessendorf, G.L. Schulz, A. Mishra, P. Kar, I. Ata, M. Weidelener, M. Urdanpilleta, J. Hanisch, E. Mena-Osteritz, M. Linden, Efficiency improvement of solution-processed dithienopyrrole-based a-d-a oligothiophene bulk-heterojunction solar cells by solvent vapor annealing, Advanced Energy Materials, 1400266, 4 (2014).
20. S. Mukherjee, C.M. Proctor, J.R. Tumbleston, G.C. Bazan, T.Q. Nguyen, H. Ade, Importance of Domain Purity and Molecular Packing in Efficient Solution-Processed Small-Molecule Solar Cells, Advanced Materials, 1105-1111, 27 (2015).
21. M. Li, F. Liu, X. Wan, W. Ni, B. Kan, H. Feng, Q. Zhang, X. Yang, Y. Wang, Y. Zhang, Subtle balance between length scale of phase separation and domain purification in small-molecule bulk-heterojunction blends under solvent vapor treatment, Advanced Materials, 6296-6302, 27 (2015).
22. Y. Akiyama, H. Tachibana, R. Azumi, T. Miyadera, M. Chikamatsu, T. Koganezawa, S. Yagi, H. Yaguchi, Effects of solvent vapor annealing on organic photovoltaics with a new type of solution-processable oligothiophene-based electronic donor material, Japanese Journal of Applied Physics, 08RE09, 57 (2018).
23. C. Jiao, C. Pang, Q. An, Nonfullerene organic photovoltaic cells exhibiting 13.76% efficiency by employing upside-down solvent vapor annealing, International Journal of Energy Research, 8716-8724, 43 (2019).
24. M. Berlinghof, S. Langner, C. Harreiß, E.M. Schmidt, R. Siris, F. Bertram, C. Shen, J. Will, T. Schindler, A. Prihoda, Crystal-structure of active layers of small molecule organic photovoltaics before and after solvent vapor annealing, Zeitschrift für Kristallographie-Crystalline Materials, 15-28, 235 (2020).
25. A.T. JG. Sánchez, VSB. Member, M. Estrada, J. Pallarès, LF. Marsal, Effects of Annealing Temperature on the Performance of Organic Solar Cells Based on Polymer: Non-Fullerene Using V2O5 as HTL, IEEE Journal of the Electron Devices Society, 421‑428, 8 (2020).
26. D. Zomerman, J. Kong, S.M. McAfee, G.C. Welch, T.L. Kelly, Control and characterization of organic solar cell morphology through variable-pressure solvent vapor annealing, ACS Applied Energy Materials, 5663-5674, 1 (2018).
27. R. Datt, A. Bagui, A. Siddiqui, R. Sharma, V. Gupta, S. Yoo, S. Kumar, S.P. Singh, Effectiveness of solvent vapor annealing over thermal annealing on the photovoltaic performance of non-fullerene acceptor based BHJ solar cells, Scientific reports, 1-10, 9 (2019).
28. Z.P. Z. Wang, Z. Xiao, D. Seyitliyev, K. Gundogdu, L. Ding, H. Adeet al Thermodynamic Properties and Molecular Packing Explain Performance and Processing Procedures of Three D18:NFA Organic Solar Cells, Advanced Materials, 1–8, 32 (2020).
29. H. Chen, J. Miao, J. Yan, Z. He, H. Wu, Improving organic solar cells efficiency through a two-step method consisting of solvent vapor annealing and thermal annealing, IEEE Journal of Selected Topics in Quantum Electronics, 66-72, 22 (2015).
30. G. Li, T. Yang, H. Cheng, Y. Zhang, J. Wang, Y. Liu, An investigation of annealing methods for benzodithiophene terthiophene rhodanine based all small molecule organic solar cells, Organic Electronics, 105904, 87 (2020).
31. F. Zhao, C. Wang, X. Zhan, Morphology control in organic solar cells, Advanced Energy Materials, 1703147, 8 (2018).
32. R.S. Gurney, D.G. Lidzey, T. Wang, A review of non-fullerene polymer solar cells: from device physics to morphology control, Reports on Progress in Physics, 036601, 82 (2019).
33. S.P. Nalawade, F. Picchioni, L. Janssen, Supercritical carbon dioxide as a green solvent for processing polymer melts: Processing aspects and applications, Progress in polymer science, 19-43, 31 (2006).
34. W.-C. Tsai, Y. Wang, Progress of supercritical fluid technology in polymerization and its applications in biomedical engineering, Progress in Polymer Science, 101161, 98 (2019).
35. N. Yousefi, B.S. Saghez, R.D. Pettipas, T.L. Kelly, L.G. Kaake, Physical supercritical fluid deposition

of polymer films: controlling the crystallinity with pressure, Materials Chemistry Frontiers, 1428-1437, 5 (2021).
36. M. Iqbal, C. Mensen, X. Qian, F. Picchioni, Green processes for green products: the use of supercritical CO_2 as green solvent for compatibilized polymer blends, Polymers, 1285, 10 (2018).
37. A. Tabernero, L. Baldino, S. Cardea, E. Martín del Valle, E. Reverchon, A phenomenological approach to study mechanical properties of polymeric porous structures processed using supercritical CO_2, Polymers, 485, 11 (2019).
38. N. Zachmann, Separation of organic components from crystalline silicon solar cells by supercritical fluid technology, (2020).
39. J.A. Amonoo, E. Glynos, X.C. Chen, P.F. Green, An alternative processing strategy for organic photovoltaic devices using a supercritical fluid, The Journal of Physical Chemistry C, 20708-20716, 116 (2012).
40. C.A. Kelly, K.L. Harrison, G.A. Leeke, M.J. Jenkins, Detection of melting point depression and crystallization of polycaprolactone (PCL) in scCO 2 by infrared spectroscopy, Polymer journal, 188-192, 45 (2013).
41. S. Grob, A.N. Bartynski, A. Opitz, M. Gruber, F. Grassl, E. Meister, T. Linderl, U. Hörmann, C. Lorch, E. Moons, Solvent vapor annealing on perylene-based organic solar cells, Journal of Materials Chemistry A, 15700-15709, 3 (2015).
42. Z.L. L. Xiao, Q. Hu, Y. Liu, W.Zhong, X. Mei, T P. Russell, Y. Liu, Y. Min, X. Peng Y. Caoet, Improving the efficiencies of small molecule solar cells by solvent vapor annealing to enhance J-aggregation, Journal of Materials Chemistry C, 9618–9624, 7 (2019).
43. M. Babics, R.-Z. Liang, K. Wang, F. Cruciani, Z. Kan, M. Wohlfahrt, M.-C. Tang, F. Laquai, P.M. Beaujuge, Solvent vapor annealing-mediated crystallization directs charge generation, recombination and extraction in BHJ solar cells, Chemistry of Materials, 789-798, 30 (2018).
44. M. Zhang, F. Zhang, Q. An, Q. Sun, W. Wang, X. Ma, J. Zhang, W. Tang, Nematic liquid crystal materials as a morphology regulator for ternary small molecule solar cells with power conversion efficiency exceeding 10%, Journal of materials chemistry A, 3589-3598, 5 (2017).
45. H. Hulkkonen, T. Salminen, T. Niemi, Automated solvent vapor annealing with nanometer scale control of film swelling for block copolymer thin films, Soft matter, 7909-7917, 15 (2019).
46. K. Gao, W. Deng, L. Xiao, Q. Hu, Y. Kan, X. Chen, C. Wang, F. Huang, J. Peng, H. Wu, New insight of molecular interaction, crystallization and phase separation in higher performance small molecular solar cells via solvent vapor annealing, Nano Energy, 639-648, 30 (2016).
47. R. Xia, C.J. Brabec, H.-L. Yip, Y. Cao, High-throughput optical screening for efficient semitransparent organic solar cells, Joule, 2241-2254, 3 (2019).
48. B. Qiu, Z. Chen, S. Qin, J. Yao, W. Huang, L. Meng, H. Zhu, Y. Yang, Z.G. Zhang, Y. Li, Highly Efficient All-Small-Molecule Organic Solar Cells with Appropriate Active Layer Morphology by Side Chain Engineering of Donor Molecules and Thermal Annealing, Advanced Materials, 1908373, 32 (2020).
49. C.V. Kumar, L. Cabau, A. Viterisi, S. Biswas, G.D. Sharma, E. Palomares, Solvent annealing control of bulk heterojunction organic solar cells with 6.6% efficiency based on a benzodithiophene donor core and dicyano acceptor units, The Journal of Physical Chemistry C, 20871-20879, 119 (2015).
50. C.L. Radford, R.D. Pettipas, T.L. Kelly, Watching Paint Dry: Operando Solvent Vapor Annealing of Organic Solar Cells, The Journal of Physical Chemistry Letters, 6450-6455, 11 (2020).
51. Z. Yi, W. Ni, Q. Zhang, M. Li, B. Kan, X. Wan, Y. Chen, Effect of thermal annealing on active layer morphology and performance for small molecule bulk heterojunction organic solar cells, Journal of Materials Chemistry C, 7247-7255, 2 (2014).
52. J.-L. Wang, K.-K. Liu, J. Yan, Z. Wu, F. Liu, F. Xiao, Z.-F. Chang, H.-B. Wu, Y. Cao, T.P. Russell, Series of multifluorine substituted oligomers for organic solar cells with efficiency over 9% and fill factor of 0.77 by combination thermal and solvent vapor annealing, Journal of the American Chemical Society, 7687-7697, 138 (2016).
53. H.Y. Güney, Z. Avdan, H. Yetkin, Optimization of annealing temperature and the annealing effect on life time and stability of P3HT: PCBM-based organic solar cells, Materials Research Express, 045103, 6 (2019).
54. S.M. Abdullah, Z. Ahmad, K. Sulaiman, The impact of thermal annealing to the efficiency and stability of organic solar cells based on PCDTBT: PC71BM, Procedia-Social and Behavioral Sciences, 2135-2142, 195 (2015).
55. W. Zhang, R. Hu, X. Zeng, X. Su, Z. Chen, X. Zou, J. Peng, C. Zhang, A. Yartsev, Effect of post-thermal annealing on the performance and charge photogeneration dynamics of pffbt4t-2od/pc71bm solar cells, Polymers, 408, 11 (2019).

56. X. Wan, Y. Liu, F. Wang, J. Zhou, G. Long, Y. Chen, Improved efficiency of solution processed small molecules organic solar cells using thermal annealing, Organic Electronics, 1562-1569, 14 (2013).
57. S.M. McAfee, A.-J. Payne, S.V. Dayneko, G.P. Kini, C.E. Song, J.-C. Lee, G.C. Welch, A non-fullerene acceptor with a diagnostic morphological handle for streamlined screening of donor materials in organic solar cells, Journal of Materials Chemistry A, 16907-16913, 5 (2017).
58. Y. Zhang, M.T. Sajjad, O. Blaszczyk, A. Ruseckas, L.A. Serrano, G. Cooke, I.D. Samuel, Enhanced exciton harvesting in a planar heterojunction organic photovoltaic device by solvent vapor annealing, Organic Electronics, 162-166, 70 (2019).
59. Y. Zheng, S. Li, D. Zheng, J. Yu, Effects of different polar solvents for solvent vapor annealing treatment on the performance of polymer solar cells, Organic electronics, 2647-2653, 15 (2014).